EBERHARD KARLS UNIVERSITÄT TÜBINGEN

BACHELOR THESIS

Subradiant routing on a Y-shaped atomic tree in free space

Author:
Leopold BODAMER

Supervisor:
Prof. Dr. Beatriz OLMOS SANCHEZ

A thesis submitted in fulfillment of the requirements for the degree of Bachelor of Science

in

Theoretical Atomic Physics and Synthetic Quantum Systems
Institut für Theoretische Physik

October 4, 2024

Declaration of Authorship

I, Leopold BODAMER, declare that this thesis titled, "Subradiant routing on a Y-shaped atomic tree in free space" and the work presented in it are my own. I confirm that:

- This work was done wholly or mainly while applying for a research degree at this University.
- Where any part of this thesis has previously been submitted for a degree or any other qualification at this University or any other institution, this has been clearly stated.
- Where I have consulted the published work of others, this is always clearly attributed.
- Where I have quoted from the work of others, the source is always given. With the exception of such quotations, this thesis is entirely my own work.
- I have acknowledged all main sources of help.
- Where the thesis is based on work done by myself jointly with others, I have made clear exactly what was done by others and what I have contributed myself.

Signed:

Date:

EBERHARD KARLS UNIVERSITÄT TÜBINGEN

Abstract

Mathematisch-Naturwissenschaftliche Fakultät
Institut für Theoretische Physik

Bachelor of Science

Subradiant routing on a Y-shaped atomic tree in free space

by Leopold BODAMER

This thesis investigates the directional routing of excitations in atomic systems using subradiant states. Building on Bottarelli's quantum router [1], this thesis adapts the model to atomic systems, addressing the challenges of controlling interactions in fully connected systems. Atom light interactions have been heavily studied for atomic lattices [2–5]. In this theis three chains, that are connected by an equilateral triangle and an isosceles triangle are studied. By allowing different dipole orientations on each chain, three distinct topologies are considered. The results show that controlling the topology and the initial state enables directional routing, where a topology with equilateral triangle and aligned dipoles emerges as the most practical for stable readout.

Acknowledgements

I would like to express my deepest gratitude to those who supported me throughout this journey. First and foremost, I sincerely thank my supervisor Prof. Dr. Beatriz OLMOS SANCHEZ for her guidance and encouragement. Her mentorship was crucial in shaping this work.
A special thanks to Marcel Cech, whose expertise and advice greatly contributed to the development of this work. I am also deeply grateful for my colleagues and fellow students, Niklas Schmidt, Paul Haffner, Ardit Thaqi, Christian Gommeringer for their assistance, which made this experience both productive and enjoyable. I would like to especially thank Niclas Schilling and Paul Haffner for proofreading this thesis. Additionally, I am thankful to Tabea Bodamer for her assistance with English grammar and to Konstanze Bodamer for her financial support. Finally, I would like to extend my appreciation to my girlfriend, Anna Schupeta, for her constant love, patience, and understanding through this process.

Contents

Chapter 1

Introduction

1.1 Motivation

One essential goal of quantum optics is to build efficient and controllable interactions between photons and atoms. A challenge for this is unwanted (spontaneous) emission, where photons are scattered into channels out of control. This spontaneous emission hampers the development of quantum technologies, especially in quantum information processing. Quantum information processing stands at the forefront of modern technological advancement. Insights into energy, and especially information transport within complex systems, are of utmost interest, as they could lead to advances in quantum routing and storage. Subradiant states are a promising concept for this field of study, since they offer ultrafast readout [6] and long lifetimes [7].

The goal of this thesis is to perform robust directional photon routing on atomic systems in free-space. Focusing on a Y-shaped atomic tree, we explore different topologies to enable long-lived information transport as a proof of concept.

1.2 Outline

This thesis is structured as follows. Chapter 2 introduces the theoretical background. It covers the concepts of open quantum systems, subradiance and superradiance, and the Green tensor. These tools are essential foundations for describing atom-atom interactions in free space, including dipole-dipole interactions and coupling to a photonic bath. The quantum router of [1] is presented and summarized in Chapter 3. It introduces the concepts of graph theory and explains how quantum evolution on a graph topology can be utilized to achieve directional routing of information. Chapter 4 will be the core of this thesis, adapting this model to an atomic system. This chapter delves into the challenges of implementing directional routing in a fully connected atomic system and investigates various solutions to control the phase of interactions. It further extends the analysis to systems with a larger number of atoms, focusing on coupling control and routing capabilities in different configurations, such as equilateral and isosceles triangles. Chapter 5 concludes the thesis by summarizing the results and discussing potential future directions in the field of quantum routing in atomic systems.

Chapter 2

Theoretical background

This chapter introduces the fundamental theory of open quantum systems. With these tools the phenomena of coherent dissipation, specifically subradiance and superradiance, in systems of interacting atoms can be described. Finally, the chapter discusses the role of the Green tensor in modeling the effects of electromagnetic interactions between atoms in these systems.

2.1 Open Quantum Systems

Every real-world quantum system S (except for the whole universe) is inevitably interacting with an environment/a bath B. This interaction introduces additional degrees of freedom that influence the system's behavior, complicating its analysis. An effective equation of motion, the so-called Lindblad "master" equation, is found for the (sub-)system of interest S. Detailed derivations of this equation can be found in [8, 9]. The main ideas are outlined here.
The combined Hamiltonian of the system is given by

$$\hat{H} = \hat{H}_{\mathrm{S}} + \hat{H}_{\mathrm{B}} + \hat{H}_{\mathrm{I}}, \tag{2.1}$$

where $\hat{H}_{\mathrm{S}}$, $\hat{H}_{\mathrm{B}}$ act only on the Hilbert spaces of S, B respectively, and $\hat{H}_{\mathrm{I}}$ describes their interaction. In the Dirac picture, a state only evolves, according to the time-evolution operator $\hat{U}$ with the non-interacting Hamiltonian $\hat{H}_0 = \hat{H}_{\mathrm{S}} + \hat{H}_{\mathrm{B}}$.
A stochastic quantum state can be described by a density matrix $\hat{\rho}$. In the Dirac (also called interaction-) picture, the evolution of the total density matrix $\hat{\rho}$ is given by the Liouville-von Neumann equation [9]

$$\frac{d\hat{\rho}(t)}{dt} = -\frac{i}{\hbar}\left[\hat{H}'_I(t), \hat{\rho}(t)\right], \tag{2.2}$$

where $\hat{H}'_I(t) = \hat{U}^{\dagger}\hat{H}_I\hat{U}$ with the time-evolution operator

$$\hat{U}(t) = \exp\left[-\frac{i}{\hbar}\left(\hat{H}_{\mathrm{S}} + \hat{H}_{\mathrm{B}}\right)t\right]. \tag{2.3}$$

The idea is to integrate Equation 2.2 and then apply the following approximations [8]. First the **Born approximation** assumes that the interaction $\hat{H}_{\mathrm{I}}$ between the bath and the system is small. The **Markov approximation**, which assumes that bath correlations decay on a much shorter timescale than any relevant dynamics of the system, allows one to write the total state at time $t = 0$ as a tensor product of two states. These correspond to the fast and slow variables $\hat{\rho} = \hat{\rho}_{\mathrm{S}} \otimes \hat{\rho}_{\mathrm{B}}$. The correlations of the bath can thus be traced out, and $\mathrm{tr}_B[\hat{H}'_I(t), \hat{\rho}(0)] = 0$. Finally, using the **secular approximation** then leads to an equation in Lindblad form by averaging over very fast oscillating terms. In the Schrödinger picture, one obtains a general "master" equation in Lindblad form

$$\frac{d\hat{\rho}_S}{dt} = -\frac{i}{\hbar}[\hat{H}, \hat{\rho}_S] + \sum_k \left(\hat{L}_k \hat{\rho}_S \hat{L}_k^\dagger - \frac{1}{2} \left\{ \hat{L}_k^\dagger \hat{L}_k, \hat{\rho}_S \right\} \right), \tag{2.4}$$

with $\hat{L}$ being the so-called jump operators. From now on $\hat{\rho} \equiv \hat{\rho}_S$ will be used to denote the density matrix of the system of interest.

2.2 Coherent dissipation

A single atom that interacts with an electromagnetic field undergoes spontaneous emission. This is characterized by the rate γ, with which the probability of finding the atom in an initially excited state decays. Such an atom can be effectively described as a two-level quantum system. This is commonly realized by tuning a laser near the resonance frequency of the atomic transition, given by $\omega_0 = ck = 2\pi c/\lambda_0$. The two-dimensional Hilbert space $\mathcal{H}$ of such a Qubit is spanned by a ground state $|g\rangle$ and an excited state $|e\rangle$.
This work extends the analysis to systems involving multiple atoms. Dicke[1] first introduced that if $N \geq 2$ quantum objects are confined in a volume comparable to the dimensionality couple to a common electromagnetic environment, collective coherent decay processes appear. These drastically change the known single atomic decay behavior. Special interferences are the reason for the so-called "Dicke sub-/ superradiance". Superradiance typically occurs when a collection of quantum emitters (such as molecules and atoms [11] or quantum dots [12]) are inverted (initially mostly excited) [13]. Then, one observes that the decay rate of the photon on the collective system Γ_{eff} is enhanced relative to that of a single atom $\Gamma_{\text{eff}} > \gamma$. This can be used to build lasers that operate with very few photons [14]. The coupled atoms here rapidly release energy within a photon burst. In contrast, Dicke subradiance represents a mechanism for creating states with extended lifetimes. The decay of an excitation is suppressed $\Gamma_{\text{eff}} < \gamma$. In this case usually a single excitation [7] is shared between closely spaced emitters. This phenomenon is of particular interest if one wants to artificially create an excitation with a very long lifetime $\tau_{\text{eff}} = 1/\Gamma_{\text{eff}} >> 1/\gamma$. However, these states are very sensitive to noise and thus tough to detect experimentally [15].

2.3 Green tensor

The classical electromagnetic Green's function $\mathbf{G}(\mathbf{r}, \mathbf{r}', \omega)$ solves the inhomogeneous Helmholtz equation [3]

$$\nabla \times \nabla \times \mathbf{G}(\mathbf{r}, \mathbf{r}', \omega) - \frac{\omega^2}{c^2} \epsilon(\mathbf{r}, \omega) \mathbf{G}(\mathbf{r}, \mathbf{r}', \omega) = \delta(\mathbf{r} - \mathbf{r}') \mathbb{1}. \tag{2.5}$$

Here $\epsilon(\mathbf{r}, \omega)$ is the dielectric function and δ is the Dirac delta function. In free space, the dielectric function $\epsilon(\mathbf{r}, \omega)$ is zero, which means that the Green tensor is analytically given. Specifically, for discrete atomic positions, one can write the Green tensor evaluated at the positions of two atoms $\mathbf{r}_\alpha$ and $\mathbf{r}_\beta$ as

[1] Robert H. Dicke (1916–1997) was a prominent American physicist who made significant contributions to several fields, including quantum optics, cosmology, and gravitation. Dicke's work from 1954 [10] laid the groundwork for understanding collective atomic behaviors and has since been fundamental in many-body quantum optics.

$$\mathbf{G}(\mathbf{x}_\gamma, k_0 = \omega_0/c = 2\pi/\lambda) = \frac{e^{ik_0|\mathbf{x}_\gamma|}}{4\pi k_0^2|\mathbf{x}_\gamma|^3}\Bigg[\left(k_0^2|\mathbf{x}_\gamma|^2 + ik_0|\mathbf{x}_\gamma| - 1\right)\mathbb{1} + \left(-k_0^2|\mathbf{x}_\gamma|^2 - 3ik_0|\mathbf{x}_\gamma| + 3\right)\frac{\mathbf{x}_\gamma \times \mathbf{x}_\gamma}{|\mathbf{x}_\gamma|^2}\Bigg], \tag{2.6}$$

describes the effects of their interactions mediated by the electromagnetic field. To shorten the expression, the separation vector $\mathbf{x}_\gamma \equiv \mathbf{r}_\alpha - \mathbf{r}_\beta$ between the emitters was used. $\mathbb{1}$ denotes the three-dimensional identity matrix. k_0 is the amplitude of the wave vector of the atomic transition.

2.4 Atomic system

The goal of this section is to apply the previous ideas to a system S of N identical two level atoms that are weakly coupled to a common radiation field (the bath B). The atoms are labeled with greek subscripts 1, ..., α, ..., N. In this work, atoms are assumed to be tightly confined in free space, and the motion of the atomic sites r_α is therefore neglected. This can be achieved by using laser-generated dipole-traps [16]. The system considers only spontaneous emission and electric dipole interactions, with each atom possessing the same two energy levels $|g\rangle$ and $|e\rangle$ (see Figure 2.1).

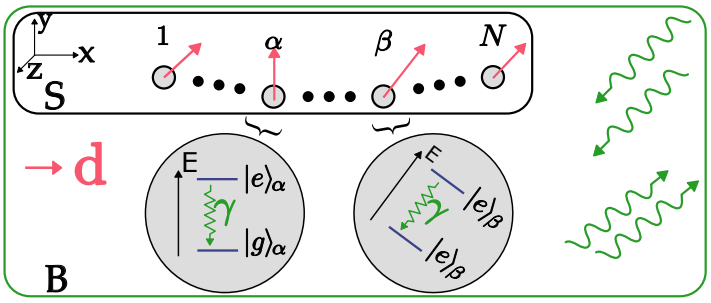

Figure 2.1: System S of N identical atoms, coupled to an electromagnetic bath B. Each carries one classical dipole-vector. It correspondes to the transition from the excited state $|e\rangle_\alpha$ to the ground state $|g\rangle_\alpha$, and points from the center of negative charge to the center of positive charge in the spatial distribution of the states.
Each atom independently is subject to spontanious emission with rate γ.

By applying the ideas of section 2.1 one obtains the quantum optical Linblad "master" equation [5]

$$\frac{d\hat{\rho}}{dt} = -\frac{i}{\hbar}[\hat{H}_{\mathrm{dd}}, \hat{\rho}] + \sum_{\alpha,\beta}\Gamma_{\alpha\beta}\left(\hat{\sigma}_\beta\hat{\rho}\hat{\sigma}_\alpha^\dagger - \frac{1}{2}\left\{\hat{\sigma}_\alpha^\dagger\hat{\sigma}_\beta, \hat{\rho}\right\}\right), \tag{2.7}$$

where the jump operators are the lowering operators σ_α for the α-th atom, while every other atom remains unchanged

$$\sigma_\alpha = |g_\alpha\rangle\langle e_\alpha| \equiv \mathbb{1} \otimes ... \otimes \mathbb{1} \otimes |g\rangle_\alpha\langle e|_\alpha \mathbb{1} \otimes ... \otimes \mathbb{1}. \tag{2.8}$$

Their Hermitian conjugates are the raising operators. The coefficients $\Gamma_{\alpha\beta}$ characterize the spontaneous emission of the system. The Hamiltonian

$$\hat{H}_{\mathrm{dd}} = -\hbar \sum_{\alpha \neq \beta} V_{\alpha\beta} \hat{\sigma}_\alpha^\dagger \hat{\sigma}_\beta \tag{2.9}$$

represents the Van der Waals interaction, an exchange of a photon between the emitters. This coupling of two atoms occurs with a rate $V_{\alpha\beta}$. Note that the sum only runs over non-equal indices. This interaction makes the atoms "distinguishable" from each other and reduces the high correlation of the pure symmetrical states, leading to the effect of subradiance in this system [11]. More specifically, the destructive interference of these oscillating dipoles is the reason for subradiance.

2.4.1 Effective Hamiltonian

Starting with Eq. (2.7), each commutator and anti-commutator is expanded, and Eq. (2.9) inserted to obtain

$$\begin{aligned}
\frac{d\hat{\rho}}{dt} &= i \sum_{\alpha \neq \beta} V_{\alpha\beta} \left(\hat{\sigma}_\alpha^\dagger \hat{\sigma}_\beta \hat{\rho} - \hat{\rho} \hat{\sigma}_\alpha^\dagger \hat{\sigma}_\beta \right) + \sum_{\alpha,\beta} \Gamma_{\alpha\beta} \left(\hat{\sigma}_\beta \hat{\rho} \hat{\sigma}_\alpha^\dagger - \frac{1}{2} \hat{\sigma}_\alpha^\dagger \hat{\sigma}_\beta \hat{\rho} - \frac{1}{2} \hat{\rho} \hat{\sigma}_\alpha^\dagger \hat{\sigma}_\beta \right) \\
&= + \left(i \sum_{\alpha \neq \beta} V_{\alpha\beta} \hat{\sigma}_\alpha^\dagger \hat{\sigma}_\beta - \frac{1}{2} \sum_{\alpha,\beta} \Gamma_{\alpha\beta} \hat{\sigma}_\alpha^\dagger \hat{\sigma}_\beta \right) \hat{\rho} \\
&\quad + \hat{\rho} \left(-i \sum_{\alpha \neq \beta} V_{\alpha\beta} \hat{\sigma}_\alpha^\dagger \hat{\sigma}_\beta - \frac{1}{2} \sum_{\alpha,\beta} \Gamma_{\alpha\beta} \hat{\sigma}_\alpha^\dagger \hat{\sigma}_\beta \right) + \sum_{\alpha,\beta} \Gamma_{\alpha\beta} \hat{\sigma}_\beta \hat{\rho} \hat{\sigma}_\alpha^\dagger .
\end{aligned} \tag{2.10}$$

The operators $\hat{V}$ and $\hat{\Gamma}$ can be introduced as

$$\hat{V} \equiv \sum_{\alpha \neq \beta} V_{\alpha\beta} \hat{\sigma}_\alpha^\dagger \hat{\sigma}_\beta, \quad \hat{\Gamma} \equiv \sum_{\alpha,\beta} \Gamma_{\alpha\beta} \hat{\sigma}_\alpha^\dagger \hat{\sigma}_\beta . \tag{2.11}$$

Using these, a non-Hermitian effective Hamiltonian $\hat{H}_{\mathrm{eff}}$ can be defined as

$$\hat{H}_{\mathrm{eff}} = \hat{V} - \frac{i}{2} \hat{\Gamma}. \tag{2.12}$$

The "master" equation describing the atomic system simplifies to

$$\frac{d\hat{\rho}}{dt} = i \left(\hat{H}_{\mathrm{eff}} \hat{\rho} - \hat{\rho} \hat{H}_{\mathrm{eff}}^\dagger \right) + \mathcal{D}(\hat{\rho}), \tag{2.13}$$

with

$$\mathcal{D}(\hat{\rho}) = \sum_{\alpha,\beta} \Gamma_{\alpha\beta} \hat{\sigma}_\beta \hat{\rho} \hat{\sigma}_\alpha^\dagger, \tag{2.14}$$

describing the Dissipation. Each operator in the master equation acts on states in the Hilbert space of dimension 2^N.

2.4.2 Dynamics in the single excitation subspace

The system is initially restricted to a superposition of single excitations $|e_\alpha\rangle \equiv |g\rangle_1 \otimes \cdots \otimes |e\rangle_\alpha \otimes \cdots \otimes |g\rangle_N$, for all $\alpha = 1, \ldots, N$. This means that exactly one, unknown atom is excited. As mentioned above, the effective Hamiltonian H_{eff} is responsible for the evolution of the initial state. Due to dissipation into the environment, the number of excitations can only decrease to zero. Consequently, the dynamics can be described within a truncated Hilbert

space spanned by the many-body ground state $|G\rangle \equiv |g\rangle_1 \otimes |g\rangle_2 \otimes \cdots \otimes |g\rangle_N$ and the single-excitation states $|e_\alpha\rangle$ [17]. A fermionic statistic with $\sigma_\alpha^\dagger |e_\alpha\rangle = 0$ holds. The dynamics in the single-excitation subspace decouple from the rest [4]. This can be seen by inserting the ansatz for the density matrix

$$\hat{\rho} = \begin{pmatrix} \hat{\rho}_{\mathrm{GG}} & \hat{\rho}_{\mathrm{Ge}} \\ \hat{\rho}_{\mathrm{eG}} & \hat{\rho}_{\mathrm{ee}} \end{pmatrix}, \tag{2.15}$$

where $\hat{\rho}_{GG} = \langle G|\hat{\rho}|G\rangle$, $\hat{\rho}_{\mathrm{Ge}} = \langle G|\hat{\rho}|e\rangle$, $\hat{\rho}_{\mathrm{eG}} = \langle e|\hat{\rho}|G\rangle$, and $\hat{\rho}_{\mathrm{ee}} = \langle e|\hat{\rho}|e\rangle$, with $|e\rangle$ being a column vector containing all single-excitation states $|e_\alpha\rangle$. Inserting this into Eq. (2.4), the equation simplifies to

$$\frac{d}{dt}\hat{\rho}_{\mathrm{ee}} = -i\left[\hat{H}_{\mathrm{eff}}\hat{\rho}_{\mathrm{ee}} - \hat{\rho}_{\mathrm{ee}}\hat{H}_{\mathrm{eff}}^\dagger\right], \tag{2.16}$$

where the operators only act on the Hilbert space of dimension N.
In this subspace, the atoms can equivalently be treated like classical dipoles [7], which justifies the usage of $\mathbf{d}$ in Figure 2.1. The dipole vector of an atom is defined by the matrix elements of the quantum mechanical dipole operator $\hat{\mathbf{d}} = q\hat{\mathbf{r}}$. The dipole vector corresponding to the transition of the α-th atom is $\mathbf{d}_\alpha = {}_\alpha\langle g|\hat{\mathbf{d}}_\alpha|e\rangle_\alpha$.
As shown, the effective Hamiltonian can be separated into the two operators $\hat{V}$ and $\hat{\Gamma}$. In the basis of the single excitation states they have a matrix representation of dimension $N \times N$. The coefficients of these matrices $(V)_{\alpha\beta}$ and $(\Gamma)_{\alpha\beta}$ can be calculated by the real and imaginary part of $\mathbf{G}$ [3]

$$V_{\alpha\beta} = \frac{\omega_\alpha^2}{\hbar\epsilon_0 c^2}\mathbf{d}_\alpha^T \mathrm{Re}[\mathbf{G}(\mathbf{r}_\alpha, \mathbf{r}_\beta, \omega_\alpha)]\mathbf{d}_\beta, \tag{2.17}$$

and

$$\Gamma_{\alpha\beta} = \frac{2\omega_\alpha^2}{\hbar\epsilon_0 c^2}\mathbf{d}_\alpha^T \mathrm{Im}[\mathbf{G}(\mathbf{r}_\alpha, \mathbf{r}_\beta, \omega_\alpha)]\mathbf{d}_\beta. \tag{2.18}$$

From now on the operator symbol $\hat{()}$ will be omitted, since a concrete matrix representation is found. The diagonal elements of Γ, $\Gamma_{\alpha\alpha} = \frac{2\omega_\alpha^2}{\hbar\epsilon_0 c^2}|\mathbf{d}_\alpha|^2 \equiv \gamma$, correspond to the single-atom decay rate. When the distance between atoms is comparable to the transition wavelength, $d \approx \lambda$, collective effects arise (see section 2.2). The off-diagonal elements satisfy $0 \leq \Gamma_{\alpha\beta} \leq \gamma$, approaching γ or zero when the interatomic distance is small or large compared to the wavelength, respectively. The diagonal elements of V are equal to zero, i.e., $V_{\alpha\alpha} = 0$ for all α. This result is expected, as the summation in Eq. (2.9) only includes terms with unequal indices ($\alpha \neq \beta$).

2.5 Tools for vizualization

This section presents the key vizualization tools. First, the reciprocal space and its importance in the analysis of periodic systems is discussed. Here the phase velocity can be designed for an effective excitation transport. A quantitative measure of the system's ability to retain excitation is layed out with the survival probability P_{sur}.

2.5.1 Reciprocal space

An infinite one-dimensional chain of atoms with aligned dipoles exhibits translational symmetry by any lattice vector $\mathbf{R}$. In such a system, all components of the Green tensor are translationally invariant. Here, Blochs theorem [18] allows the diagonalization of $\mathbf{G}$ via a

Fourier transformation. This way the eigenfunctions of **G** can be expressed as plane waves

$$|k_i\rangle = \frac{1}{\sqrt{N}} \sum_{\alpha=1}^{N} \langle e_\alpha | k_i \rangle |e_\alpha\rangle = \frac{1}{\sqrt{N}} \sum_{\alpha=1}^{N} e^{ik_i |\mathbf{r}_\alpha|} |e_\alpha\rangle. \tag{2.19}$$

The Fourier transformation can be written in matrix form as

$$T \equiv \left[|k_1\rangle \dots |k_i\rangle \dots |k_N\rangle \right], \tag{2.20}$$

where $|k_i\rangle$ denotes the i-th eigenstate corresponding to the eigenvalue G_{k_i} in reciprocal (k)-space. With each eigenvalue one can directly connect a pseudo momentum in the first Brillouin zone $k_i \in [-\pi/d, \pi/d] \subset \mathbb{R}$. This reducibility comes from the fact that each state $|k\rangle$ is unique up to a constant reciprocal lattice vector $|\mathbf{K}| = 2\pi/\mathrm{d}$. Here d is the distance of two neighboring atoms. The real and imaginary part of the eigenvalues is directly proportional to the eigenvalues V_k and Γ_k respectively (see Eqs. (2.17) and (2.18)). This relationship reveals regions of superradiance and subradiance, remember that superradiant modes correspond to $\Gamma_k > \gamma$, while subradiant modes correspond to $\Gamma_k < \gamma$. Notably, subradiance typically occurs at the boundaries of the Brillouin zone, away from its center. These modes are challenging to create experimentally due to their location in k-space [5].

2.5.2 Survival probability

Consider the Schrödinger equation for a time-independent Hamiltonian H. The time evolution of an initial state $|\psi(0)\rangle$ is given by

$$|\psi(t)\rangle = \exp\left(-\frac{i}{\hbar} H t\right) |\psi(0)\rangle. \tag{2.21}$$

For the system of N atoms, as discussed in the previous section, the initial state (assuming pure states, where $\rho_{ee} = |\psi(t)\rangle\langle\psi(t)|$) evolves under the non-Hermitian Hamiltonian H_{eff} (see Eq. (2.12)). This leads to

$$|\psi(t)\rangle \propto \underbrace{\exp(-iVt)}_{\text{Phase}} \underbrace{\exp(-\frac{\Gamma}{2}t)}_{\text{Decay}} |\psi(0)\rangle. \tag{2.22}$$

Here the Baker–Campbell–Hausdorff formula was used to seperate the operators.

The equation for the density matrix is trace-preserving ($\mathrm{Tr}[\rho] = 1$) and ρ_{GG} increases over time due to the dissipative dynamics. Therefore, the survival probability, describing the probability for not emitting a photon into the radiation field, is given by the norm of the state described by Eq. (2.22) and can be written as

$$P_{\text{sur}}(t) = ||\psi(t)\rangle|^2 = \sum_{\alpha=1}^{N} |c_\alpha(t)|^2. \tag{2.23}$$

where $|c_\alpha(t)|^2$ represents the probability amplitude of the α-th atom being excited at time t. Thus, the survival probability quantifies how the system retains its excitation as it evolves, reflecting the decay dictated by Γ.

2.5.3 Group velocity

This section directly builds on the previous two. With Eq. , one can argue that only the V matrix defines the spectrum of the effective Hamiltonian. By diagonalizing V, one can extract the eigenenergies V_k. The Phase φ of the evolved state in Eq. (2.22) is given by

$$\varphi(t) \equiv V_k t + \varphi_0 \tag{2.24}$$

where φ_0 denotes the phase of the initial state $|\psi(0)\rangle$. The group velocity v_g is thus proportional to the eigenenergies

$$v_g \propto \nabla\varphi \equiv \nabla V_k \cdot t, \tag{2.25}$$

This approach also holds as a good approximation for large but finite systems. The gradient of the spectrum, V_k, determines the dispersion relation, which ultimately depends on atomic positions and dipole orientations.
Without loss of generality, a wave-packet can be localized in k-space. For instance a Gaussian wave packet in k-space also remains Gaussian in real space after a Fourier transform. By controlling the shape of the wave packet in k-space, one can manipulate the behavior of excitation on the atoms.
One application of this is to trap photons on specific lattice sites through a flat dispersion [5]. Another application involves initializing the wave packet in a region of k-space with an approximately linear dispersion relation. In this scenario, the wave packet propagates with a nearly constant group velocity, avoiding dispersion during its evolution [4]. By tuning the atomic chain's structure and selecting appropriate initial conditions for the wave packet, one can effectively control the phase velocity and, consequently, the dynamics of the system.

Chapter 3

Presentation of the basis of this work

This thesis is based on the paper [1] by Botarelli. A quantum router on the topology of a graph with six nodes (see Figure 3.1) was analyzed and will be explained in this chapter. In the next chapter this will be adapted to an atomic system.

Graphs are mathematical structures used to model pairwise relations between N nodes. In this context, nodes represent quantum objects and edges represent interactions between them. A classical information is defined as an excitation of one of the nodes. The node-basis trivially corresponds to the Euclidean basis

$$|i\rangle \equiv (0, \ldots, \underbrace{1}_{i}, \ldots, 0)^T, \text{ for } \alpha = 1, ..., N. \tag{3.1}$$

indicating a alassical excitation of the i-th node. Quantum mechanically it would be the superposition of excitations of nodes. A Laplacian matrix L encodes the connectivity of a classical graph. Bottarelli's work extends the Laplacian matrix to allow for complex entries, resulting in a hermitian Hamiltonian H. The interactions between two nodes is the complex conjugate of the reverse interaction. The topology that was analyzed is depicted in Figure 3.1 and can be described by the 6×6 matrix

$$H^1 = \begin{pmatrix} 0 & 1 & 0 & 0 & 0 & 0 \\ 1 & \gamma & e^{-i\theta/3} & 0 & e^{i\theta/3} & 0 \\ 0 & e^{i\theta/3} & \gamma & 1 & e^{-i\theta/3} & 0 \\ 0 & 0 & 1 & 0 & 0 & 0 \\ 0 & e^{-i\theta/3} & e^{i\theta/3} & 0 & \gamma & 1 \\ 0 & 0 & 0 & 0 & 1 & 0 \end{pmatrix}, \tag{3.2}$$

where specific edges carry a phase given by θ. This means the quantum mechanical time evolution can be used to evolve an excitation ($|\psi(t = 0)\rangle = \sum_{\alpha=1}^{6} c_\alpha(t = 0)|\alpha\rangle$) on the system. The evolution breaks the time-inversal symmetry, one says it is chiral, because of the phase in the Hamiltonian. This key parameter is obtained when going along the loop in the graph Figure 3.1. It is the only quantum part of this analysis, enabling directional routing of information [19].

Figure 3.2 shows, that a phase dependant directional transport of the classical state $|\psi_0\rangle = |1\rangle$ is possible and robust. After a time T a high probability can be achieved to route the initial state into one of the nodes $|5\rangle/|6\rangle$ while a low probability of being routed into the other nodes $|6\rangle/|5\rangle$ is guaranteed.

The phase in the triangle is not necessary to be equally distributed along the three connections. The evolution is only dependent on the total phase θ. However, a symmetrical allocation makes analytical calculations manageable.

[1] The labels of the nodes 4 and 5 were switched in this definition, to be consistend with the definition of the system used later in this thesis. Such a relabeling has no effect on the physical properties.

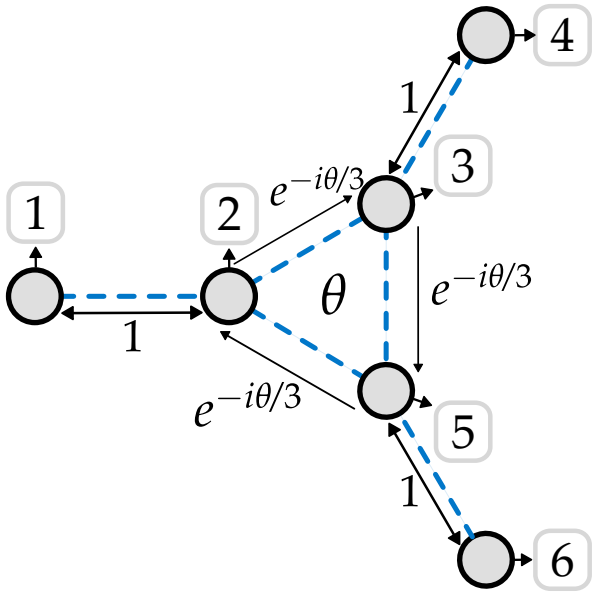

Figure 3.1: The minimal graph of the quantum router in [1]. The circles correspond to nodes, labeled from 1 to 6, and the arrows indicate edges, the interaction between the nodes. The edges with a phase point only in one direction, because the interaction is not symmetric. The inner loop carries weights that add up to a phase θ. Eq. (3.2) describes the graph interely.

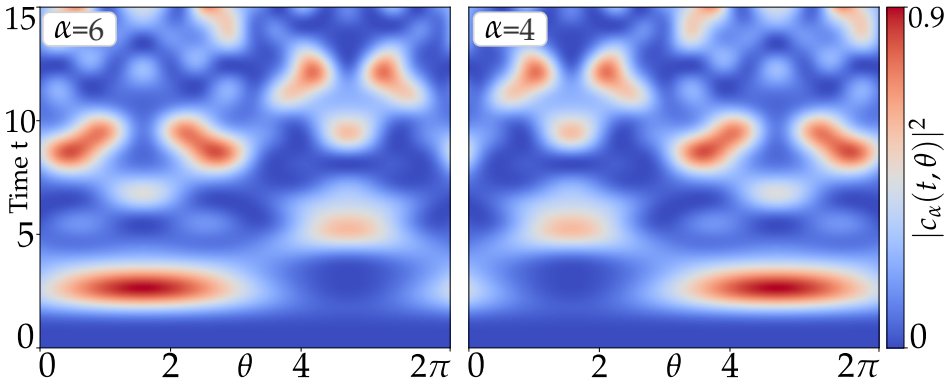

Figure 3.2: The probabilities $|c_\alpha(t)|^2$ with $c_1(0) = 1$ plottet against time t and the total phase θ of the loop in Figure 3.1.

Chapter 4

Adaptation of Botarellis work to atoms

Attempting to directly apply the ideas from Botarelli's work to a system of six atoms, as outlined at the beginning of this chapter, proves to be unsuccessful. Instead, a slightly modified approach will be developed and subsequently extended to N atoms later in this chapter.

4.1 Challenges

The atomic system (see section 2.4) is fully connected, meaning that every atom interacts with every atom. Botarelli's topology only has edges between adjacent nodes. But simplifying the atomic dynamics by working with nearest-neighbor interactions (NN) can lead to the matrix Γ having negative eigenvalues, resulting in an unphysical increase in the survival probability (see Eq. (2.22)). Consequently, the exact quantum router proposed in Botarelli's paper cannot be adopted to an atomic system.
A similar phase as in Figure 3.1 can be defined and effectively influenced by the atomic separation and the orientation of their dipoles.

4.1.1 Phase control

The entries of the effective Hamiltonian $H_{\text{eff},\alpha\beta}$ from Eq. (2.12) are complex numbers, which connect the two atoms with indices α and β. A phase $\Phi_{\alpha\beta}$ of the complex number, defined as the polar angle in the complex plane, can be extracted analytically as

$$\Phi_{\alpha\beta}(\mathbf{r}_\alpha, \mathbf{r}_\beta, \mathbf{d}_\alpha, \mathbf{d}_\beta) \equiv \arctan\left(\frac{\Gamma_{\alpha\beta}}{2V_{\alpha\beta}}\right), \tag{4.1}$$

where $\mathbf{r}_{\alpha,\beta}$ are the separation between the two atoms and $\mathbf{d}_{\alpha,\beta}$ their dipoles as defined in section 2.4. The phase $\Phi_{\alpha\beta}$ can be influenced by these parameters, since both matrices $\Gamma_{\alpha\beta}$ and $V_{\alpha\beta}$ depend on these parameters. Figure 4.1 illustrates this dependance for a system of two atoms.

Dipoles with arbitrary orientations are permitted, which is shown on the right side of Figure 4.1.
The number of atoms is increased to $N = 3$. A triangular configuration of the atoms is possible, which can be identified as the loop shown in Figure 3.1. To characterize the interactions within this triangle, the total phase θ

$$\theta \equiv \theta(\mathbf{r}_1, \mathbf{r}_2, \mathbf{r}_3, \mathbf{d}_1, \mathbf{d}_2, \mathbf{d}_3) \equiv \Phi_{12} + \Phi_{23} + \Phi_{31}, \tag{4.2}$$

is defined, which represents the phase accumulated around the triangle. This phase depends on the positions and dipole orientations of the three atoms. From this point onward, the dipoles are assumed to lie within the plane of the atoms.

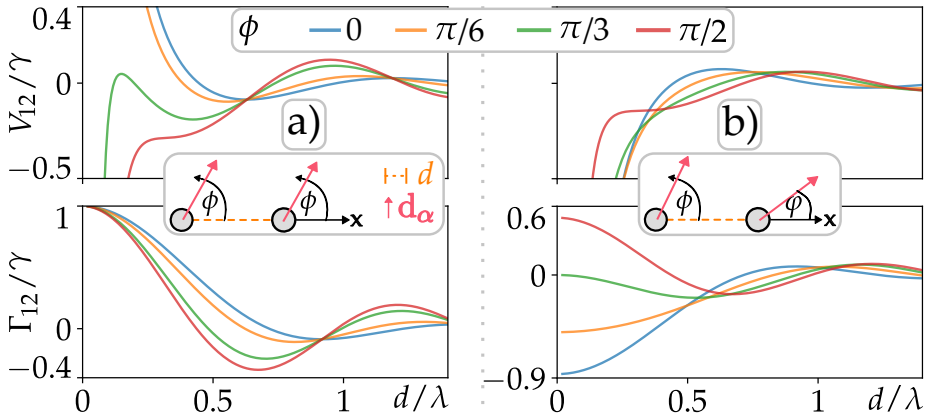

Figure 4.1: The matrix element V_{12} aswell as Γ_{12} represents the interaction strength between two atoms (dipole-dipole aswell as dissipation). They are plotted in units of γ against their separation d for different angles ϕ, which is measured with respect to the x-axis. **a)** Both dipoles are aligned. **b)** One dipole is fixed at $\varphi = 5\pi/6$ and one is vaired.

The phase can be efficiently changed by adjusting the atomic separations along the triangle. However, directional routing is not possible as can be seen in section A.1 in the Appendix. Mathematically, this system shows no chirality. This is because the Hamiltonian of the system is non-hermitian. In the following sections, the topology will be modified to accommodate this complexity.

4.2 Conditions for directional routing

Directional routing is not inherently possible with the current setup, but a configuration in which the couplings within the triangular topology favor a specific direction can be identified. For this discussion, we will focus on routing the excitation from the left into the upper arm. Due to the system's symmetry along the x-axis, the results can be mirrored to achieve routing toward the lower arm as well. To route an excitation into the upper arm, the matrix entries should satisfy the conditions

$$\frac{V_{13}}{V_{12}} \ll 1 \quad \text{and} \quad \frac{V_{23}}{V_{12}} \ll 1. \tag{4.3}$$

As described in Figure 4.1, changing the dipole orientation of different atoms modifies the elements $V_{\alpha\beta}$. This modification can be helpful in meeting the conditions specified in Eq. (4.3). To explore this further, three topologies are investigated, illustrated in the upper part of Figure 4.2. For bigger systems, additional atoms $N \geq 6$ are placed outside the triangle on extended lines between the center of the triangle and the edge atoms. The distances of these "outer" atoms are fixed at d_{ext}, while the inner distance d is varied.
The lower part of Figure 4.2 shows that the two configurations with aligned dipoles (**a)** and **c)**) have a clear optimal distance, while **b)** offers overall smaller values of the sum.
In the completely symmetric system (Figure 4.2 **a)**), the optimal angle is $\phi_{\text{opt}} = 30.04°$ with an optimal distance of $d_{\text{opt}} = 0.12\lambda$. For case two (**b)**) the optimal angles are $\phi_{\text{opt,1}} = 32.08°$, $\phi_{\text{opt,2}} = 29.63°$, and $\phi_{\text{opt,3}} = 29.12°$, with an optimal distance of $d_{\text{opt}} = 0.13\lambda$. For the isosceles triangle (**c)**), the optimal angle is $\phi_{\text{opt}} = 31.69°$ and the optimal distance is $d_{\text{opt}} = 0.09\lambda$. These values will be used in the subsequent analysis.

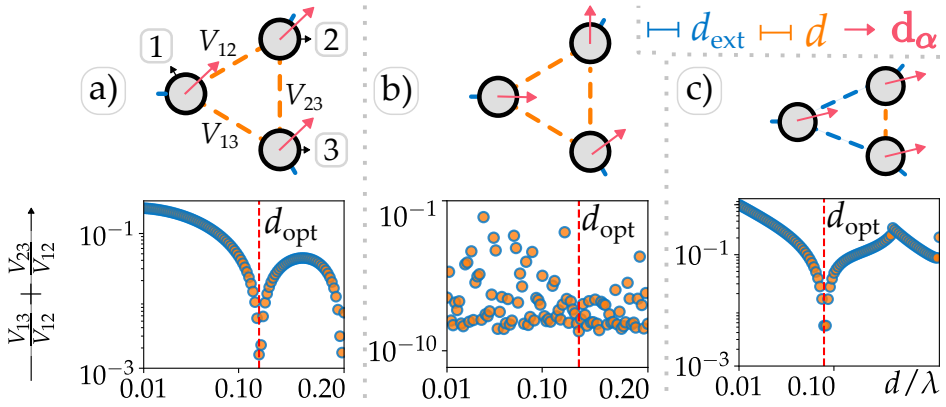

Figure 4.2: a) Equilateral triangle with aligned dipoles. **b)** Equilateral triangle with unique dipole orientations. **c)** Isosceles triangle, where one inner distance is changed and the dipoles are aligned. Each system will be investigated with $N > 6$ later, indicated the small blue connections at each atom. **Conditions:** For each distance d, there exists a set of dipole orientations, such that the ratios (Eq. 4.3) are minimal. The sum of these ratios is plotted with a logarithmic scaling against d in units of λ. Additionally, each topology offers one distance d_{opt}, where the sum is minimal. An external distance of $d_{\text{ext}} = 0.1$ was used.

4.3 Implementation of Botarelli's system with six atoms

With the optimal configurations identified, the topology proposed in Botarelli's paper [1] can be implemented with six atoms. Using the just determined angles in the case of a equilateral triangle with aligned dipoles, the dipole of atom 2 is oriented directly towards atom 3. This arrangement is visualized in Figure 4.3 **a)**.
Part **b)** shows the evolution of a initial state on the left arm. The probability of finding the photon oscillates between the atoms (1,2) and (3,4). The probability of being on atoms (5,6) is close to zero for all times. The lifetime of the photon being on the system is enhanced such that after $T = 15/\gamma$, the survival probability is 0.43. This can further be amplified by using more $N > 6$ atoms [7]. This is why an initial state with a large number of atoms will now be defined.

4.4 System definition with $N > 6$

As discussed in section 2.5.3, the procedure for a given topology of N atoms in a specific arrangement with given dipole orientations is as follows. First, the spectrum of the system is analyzed. The Hamiltonian of a finite system cannot exactly be diagonalized with a Fourier Transformation. However, it is still useful to operate in quasi-momentum space (see section A.2 in the Appendix), as discussed in section 2.5.1. In this space, a Gaussian wave packet is initialized on a subradiant branch ($\Gamma_k < 1$) with an approximately constant group velocity. A phase multiplication is then applied to determine the center of the wave packet in real space. The state in real space can be obtained by applying the inverse Fourier transform (see Eq. (2.20)) to the state in k-space. This resulting state maintains a Gaussian shape and is expressed as:

$$|\psi_x(t=0)\rangle = \sqrt{\frac{\sigma_k}{\sqrt{2\pi}}} \sum_{\alpha=1}^{N} e^{-ik_s(\alpha-\nu)} e^{-\frac{((\alpha-\nu)^2) d_{\text{ext}}^2}{4\sigma_k^2}} |e_\alpha\rangle \equiv \sum_{\alpha=1}^{N} c_\alpha(t)|e_\alpha\rangle. \tag{4.4}$$

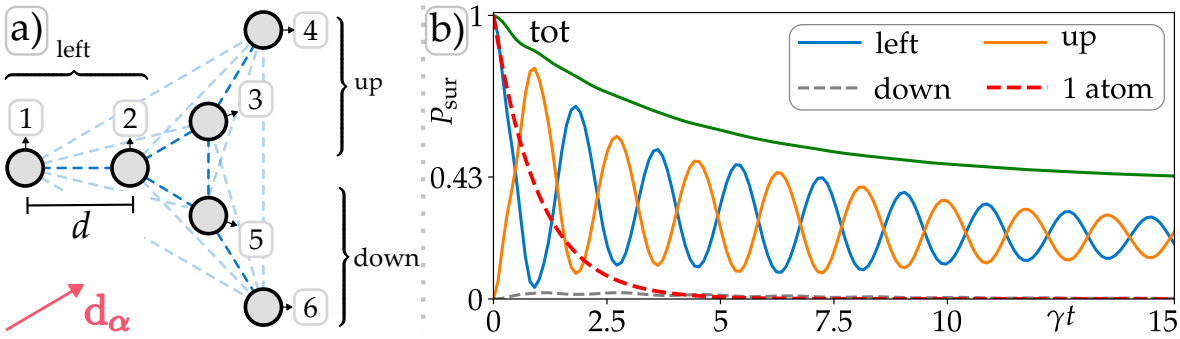

Figure 4.3: a) A fully connected system of $N = 6$ atoms, which is maximally symmetric, mimicing the topology in Figure 3.1. The opacity of a connection represents its strength, that depends on the distance between two atoms. The inner triangle is equilateral. All dipoles are aligned indicated by d_α. The system is initially in a superposition of atom 1 and 2 being excited. The state can mathematically be described by $|\psi_x(0)\rangle = [z, -z, 0, 0, 0, 0]$, with $z = 0.1701 - 0.6863i$. **b)** Probability of finding the photonic excitation plotted against γ^{-1}. The total (**"tot"**) survival probability is displayed in green, while **"left"** means the probability of being on atoms (1,2), **"up"** refers to atoms (3,4), and **"down"** corresponds to atoms (5,6). As a reference, the red dashed line shows the single atomic behavior.

In this expression, ν represents the index of the center atom in the atomic chain. In k-space the wave packet has a peak at k_s. The width of the wave packet in k-space is given by σ_k. The parameter d_{ext} denotes the atomic separation in the chain. Finally $|e_\alpha\rangle$ refers to the α-th atom being excited, which is representing the position basis.

4.4.1 Transport

The procedure for defining the initial state defined by Eq. (4.4) and its evolution is illustrated for a finite one-dimensional chain of $N = 100$ atoms in Figure 4.4.
The wave packet is reflected at the chain end and slightly disperses. When this happens, the survival probability is significantly reduced. For the evolution in the bulk, the survival probability stays approximately constant with time.
In the topology of interest the N atoms are arranged into three distinct chains shown in Figure 4.5. The left chain (left) consists of atoms numbered from 1 to $N/3$, the upper chain (up) comprises atoms numbered from $N/3 + 1$ to $2N/3$, and the lower chain (down) includes the remaining atoms from $2N/3 + 1$ to N. For the case of unique dipoles, the atoms on the left, up, down chain all have their own dipole angle $\phi_{\text{opt},1,2,3}$ respectively. Within the chain, they are aligned. The wave packet will only be initialized on the left chain. All coefficients $c_\alpha : N/3 < \alpha \leq N$ of the state $|\psi_x(t = 0)\rangle$ are set to zero.
The same procedure applied to a single chain can be used here. The shape of the spectrum depends on both the atomic distance and the dipole orientations of the left chain. Three systems with N atoms and the inner triangles according to Figure 4.4 **a)**,**b)** and **c)** are used. For cases **a)** and **b)**, the optimal inner distance is used for the external distance as well, unless otherwise noted. In contrast, with case **c)** an external distance of $d_{\text{ext}} = 0.1\lambda$ is used. Generally, the group velocity in the subradiant regime increases as the atomic distance in the chain decreases. Therefore, a smaller choice of d_{ext} results in a faster propagation of the wave packet along the chain, allowing it to reach the inner triangle more quickly.

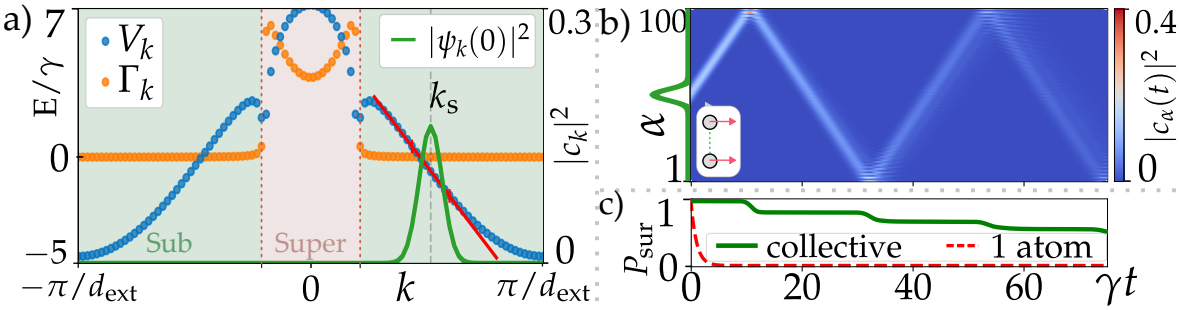

Figure 4.4: The dipoles are perpendicular to the chain of $N = 100$ atoms. **a)** Spectrum (V_k), Eigen-Decay modes (Γ_k) and norm of the wave packet $|\psi_k(0)|^2$ in momentum space are plotted against the pseudo momentum k. The regions of sub- and super radiance ($\Gamma_k < 1/ > 1$) are shaded in green / red respectively. Here a interatomic distance of $d_{ext} = 0.1\lambda$ was used. The wave packet in k space has a width of $\sigma_k = 0.05\frac{\pi}{d_{ext}}$ around $k_s \approx 0.5\frac{\pi}{d_{ext}}$. A straight (red line) has been fitted through to modes V_k over a range $[k_s \pm 2\sigma_k]$ indicating a linear regieme in V_k. **b)** The initial state$|\psi_x(t = 0)\rangle$, depicted as a green line left of the color plot is evolved. The probabily of being on the α-th atom against time is plotted in units of γ^{-1}. **c)** The survival probability plotted against time in units of γ^{-1}. The green line indicates the total, collective survival probability and the dashed red line indicates the single atom decay as a reference.

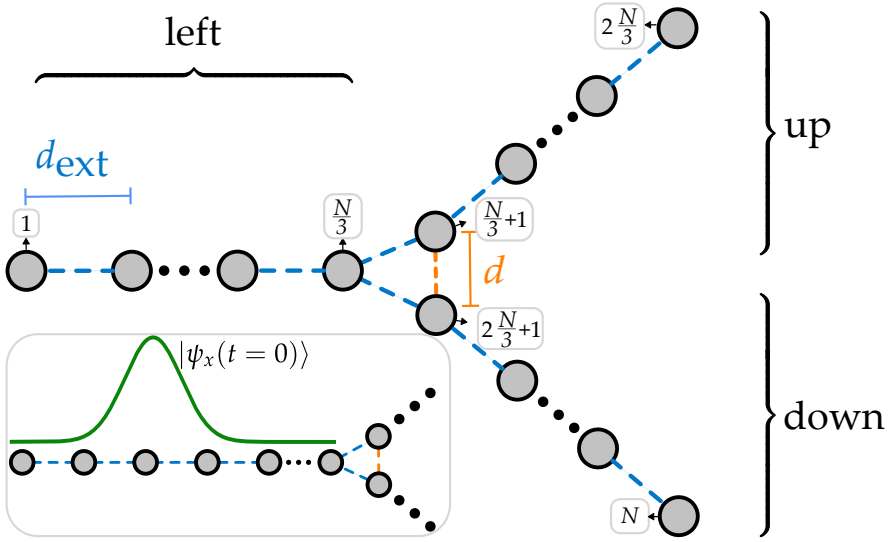

Figure 4.5: Setup for N atoms with an isosceles inner triangle. The initial state is a Gaussian, localized near the center of the left arm as indicated by the green line. Full connectivity is omitted for visual clarity, although every atom interacts with every other atom. A similar arrangement can be made with an equilateral triangle.

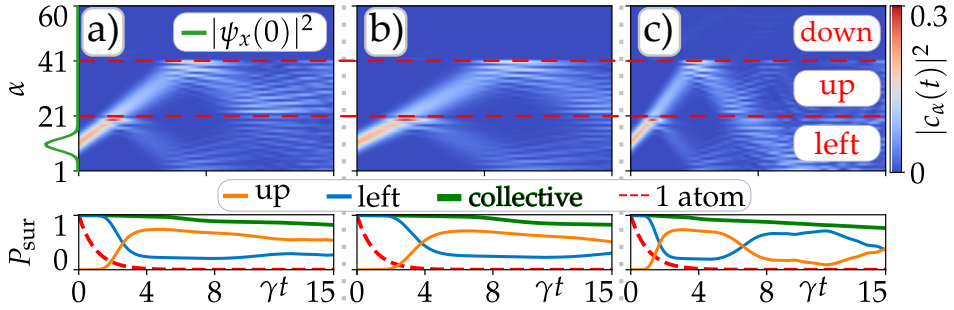

Figure 4.6: System with $N = 60$ atoms. **a)** Equilateral triangle with aligned dipoles. **b)** Equilateral triangle with unique dipoles. **c)** Isosceles triangle with aligned dipoles. For each system the same initial state $|\psi_x(t=0)\rangle$, depicted as a green line left of the first color plot is evolved. The optimal setups (see section 4.2) are used, with $\sigma_k = 0.08\frac{\pi}{d_{ext}}$ and $k_s \approx 0.58\frac{\pi}{d_{ext}}$. The probabily of being on the α-th atom against time is plotted in units of γ^{-1}. The lower plots show the survival probability (**"tot"** in green, **"left"**, **"up"** shows the probability of finding the photonic excitation on the atoms of the left, upper chain respectively. This time **"down"** is not shown. As a reference, the red dashed line shows the single atomic behavior.

When the wave packet encounters the triangle, a transmission (T), reflection (R), and a small leakage (L) are expected.These coefficients can be defined as

$$T = \frac{P_{\text{up}(t=T)}}{P_{\text{left}(t=0)}}, \quad R = \frac{P_{\text{left}(t=T)}}{P_{\text{left}(t=0)}} \quad \text{and} \quad L = \frac{P_{\text{down}(t=T)}}{P_{\text{left}(t=0)}}. \tag{4.5}$$

Here, $t = T$ represents a point in time after the routing event when each part of the original wave packet is far away from the triangle. With this, one can measure the effectiveness of routing in the different topologies.

4.5 Routing in systems with $N = 60$ atoms

Starting from $N = 60$, a wave packet that does not couple to any superradiant modes and have a well defined center in real space can be initialized on the system. The evolutions for this case are shown in Figure 4.6.
In this minimal example, the survival probability after $T = 15/\gamma$ is 0.82, 0.83, and 0.77 for topologie **a)**, **b)**, **c)** respectively. An observable dispersion occurs indicating that a larger atomic number is necessary to achieve more robust routing. Table 4.1 presents the reflection, transmission, and leakage coefficients for the three topologies.

Table 4.1: Reflection R, Transmission T, and Leakage L coefficients for three topologies with $N = 60$. Here, 'E' stands for equilateral geometry, and 'I' stands for isosceles geometry

Case	R	T	L
E, aligned ($T = 4/\gamma$)	22.97	73.99	1.01
E, unique ($T = 6/\gamma$)	25.68	71.59	0.46
I, aligned ($T = 3/\gamma$)	20.38	73.73	2.82

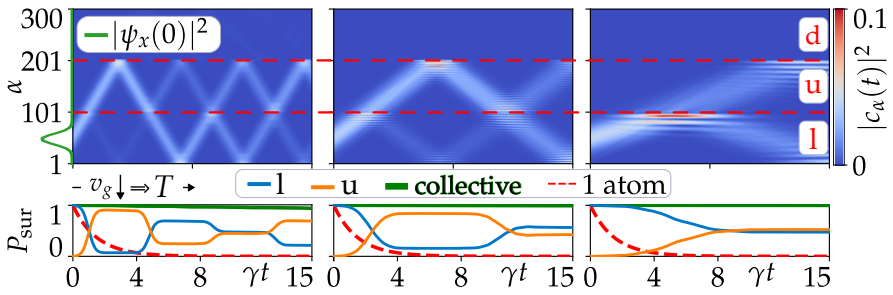

Figure 4.7: Evolution for an system with $N = 300$ and an equilateral triangle with unique dipoles. The distance is chosen to be $d \approx 0.05\lambda$ and the corresponding angles $\phi_{1,2,3} = [22.12°, 38.56°, 29.68°]$ are extracted from Figure 4.2. The same quantities as in Figure 4.6 are plotted for different initial states. The wave packet is centered around $k_s = 0.43, 0.79, 0.92 \frac{\pi}{d_{\text{ext}}}$ from left to right and $\sigma_k = 0.01 \frac{\pi}{d_{\text{ext}}}$.

As shown in Table 4.1, the reflection and transmission coefficients vary slightly across the cases. The equilateral topology with unique dipoles has the highest reflection coefficient, while the totally symmetric (equilateral, aligned) and isosceles topologies exhibit slightly higher transmission. Leakage into the lower arm remains relatively small across all configurations, with the isosceles topology showing the highest leakage of $L = 2.82$. Overall, these results suggest that while the equilateral triangle with unique dipoles can maximize reflection, other configurations might offer a better transmission control. Since the three cases have slightly different interatomic distances d_{ext}, the group velocity changes. This results in the fastest transmission for the isosceles case and the slowest for the equilateral case with unique dipoles. At equal external distances of 0.1λ, only small deviations are expected to stem from the different dipole orientations on the chains. The data is collected at different time points, because the group velocity is different for each case.

4.6 Routing in systems with $N = 300$ atoms

In the equilateral triangle configuration with unique dipoles, the coupling ratios are very small for many distances within the studied range. For example the distance $d = 0.05\lambda \neq d_{\text{opt}}$ also fulfills the conditions very good. Using a wave packet with a center in k-space closer to the Brillouin zone boundary results in a smaller group velocity is now analyzed. For this analysis the distance $d_{\text{ext}} = 0.05\lambda$ is chosen. It enables a faster propagation of the photon on the chains.
As can be seen in Figure 4.7, a higher group velocity results in a more profound routing. As k_s decreases, the group velocity v_g increases because the dispersion is steeper at the Brillouin zone center. As a result, the transmission decreases. This comes at the cost of a higher dissipation, which can be seen since the collective survival probability P_{sur} decreases slightly fast for lower k_s. This makes sense, because the Brillouin zone center corresponds to the superradiant regime (see Figure 4.4). The most subradiant mode decreases with the systems size $\Gamma_{k,\text{min}} \propto N^{-3}$ [7].
Table 4.2 presents the reflection, transmission, and leakage coefficients for varying values of k_s. As k_s increases, the reflection coefficient (R) also increases, while the transmission coefficient (T) decreases. This indicates that a higher group velocity, associated with smaller k_s favors transmission.

The symmetric topology, the equilateral triangle with unique dipoles, and isosceles triangle,

Table 4.2: The dependence of k_s on R, T, and L for $N = 300$ and an equilateral triangle with unique dipoles

Case	R	T	L
$k_s = 0.43\frac{\pi}{d_{ext}}$ $(T = 1/\gamma)$	8.58	89.28	1.92
$k_s = 0.79\frac{\pi}{d_{ext}}$ $(T = 3/\gamma)$	15.73	84.02	0.00
$k_s = 0.92\frac{\pi}{d_{ext}}$ $(T = 7/\gamma)$	47.62	52.28	0.00

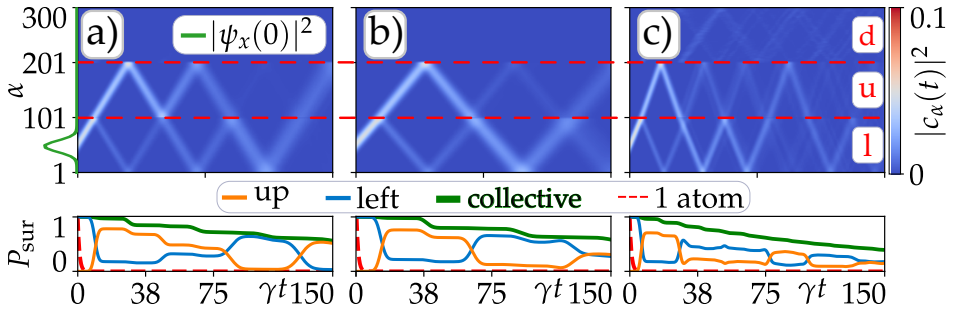

Figure 4.8: Evolution for $N = 300$ with $\sigma_k = 0.02\frac{\pi}{d_{ext}}$ and $k_s \approx 0.5\frac{\pi}{d_{ext}}$. This figure shows similar plots as in Fig. 4.6 for the optimal configurations: **a)** Symmetric topology, **b)** Equilateral triangle with unique dipoles, and **c)** Isosceles triangle with aligned dipoles.

have provided a comprehensive understanding of how the group velocity, atomic distance, and dipole orientations influence the transmission. These insights are now applied to a system of $N = 300$ atoms, as shown in Figure 4.8. The center of the wave packet k_s is chosen as a balance between dissipation and fast propagation.
For all triangle types, the wave packet primarily transmits into the upper arm, with variations in reflection into the left arm and leakage into the lower arm.The reflection (R), transmission (T), and leakage (L) coefficients for each setup are highlighted in Table 4.3

Table 4.3: Reflection (R), Transmission (T), and Leakage (L) coefficients for different topologies with $N = 300$ at $k_s \approx 0.5\frac{\pi}{d_{ext}}$.

Topology	R	T	L
E, aligned $(T = 20/\gamma)$	17.84	78.22	1.17
E, unique $(T = 20/\gamma)$	22.30	75.68	0.04
I, ligned $(T = 15/\gamma)$	17.90	70.77	7.49

The equilateral triangle generally exhibits higher transmission and lower reflection compared to the isosceles triangle, with minimal leakage. In the equilateral triangle, the wave packet components that split at the triangle effectively overlap when they encounter the triangle again. This results in a more consistent group velocity along each chain, enhancing overall transmission and reducing leakage. Each encounter with a chain's edge results in a small dip in survival probability, similar to a single chain scenario. For the isosceles triangle, these dips occur more frequently, reducing the survival probability over time. The smaller chain distances in this topology increase the group velocity, leading to more reflections and consequently higher losses. This results in the lowest survival probability among the topologies studied, with notable leakage into the lower arm. The completely symmetric topology demonstrates the highest stability, with no significant leakage and a relatively high

transmission coefficient. The setup with unique dipole orientations offers similarly good results; however, it is not physically achievable in practice. Therefore, the equilateral triangle with aligned dipoles is more relevant for stable readout. The isosceles triangle is suitable for faster readout at the cost of an increased leakage.

Chapter 5

Conclusion

This thesis explored the feasibility of directional routing of excitations in atomic systems using subradiant states. Starting from Bottarelli's quantum router model, the work was adapted to atomic systems, addressing the challenges of controlling interactions in the fully connected setups. Directionality in the classical sense was not possible, since the atomic Hamiltonian is not Hermitian. It was necessary to modify Bottarelli's initial approach for routing.

By modifying both the atomic distance and dipole orientations, three different triangular topologies were investigated: The equilateral triangle with aligned dipoles, the equilateral triangle with unique dipoles, and the isosceles triangle. It was shown that controlling these parameters allows a "brute-force" directional routing of excitations in the atomic system by minimizing specific dipole-dipole couplings in the triangle.

The topology with unique dipole orientations showed a very high transmission coefficient of $T \approx 90$ for very closely spaced atoms $d_{\text{ext}} = d = 0.05\lambda$. But this setup is hard to prepare experimentally as one would need an inhomogeneous external field applied to the apparatus. The routing for the optimal distances around $d_{\text{ext}} = 0.1\lambda$ was demonstrated to be most effective when the group velocity of the wave packet is approximately $\pi/(2d_{\text{ext}})$. The equilateral triangle with aligned dipoles emerges as the most viable solution for stable transmission of $T \approx 78$ in experimental setups, fitting with Bottarelli's original topology.

For larger atomic systems, routing effectiveness improves. The results also suggest that an isosceles triangle is suited for faster readout, though this comes at the cost of higher leakage into the unwanted chain.

In summary, this work provided a framework for achieving directional routing in atomic systems. Future research could investigate the implementation of these findings in experimental conditions. It would also be interesting to see whether similar directional routing can be achieved in systems with multiexcitation states.

Appendix A

Extra material

A.1 No directionality

For N = 6 one can recreate the topology as in Figure 3.1. The phase θ depends on the positions and dipole orientations of the three loop-atoms. This dependance is shwon in Figure A.1 a). Multiple combinations that lead to the same θ have different evolutions, which is depicted in Figure A.1 b). Changing the phase does not allow for directional routing. A

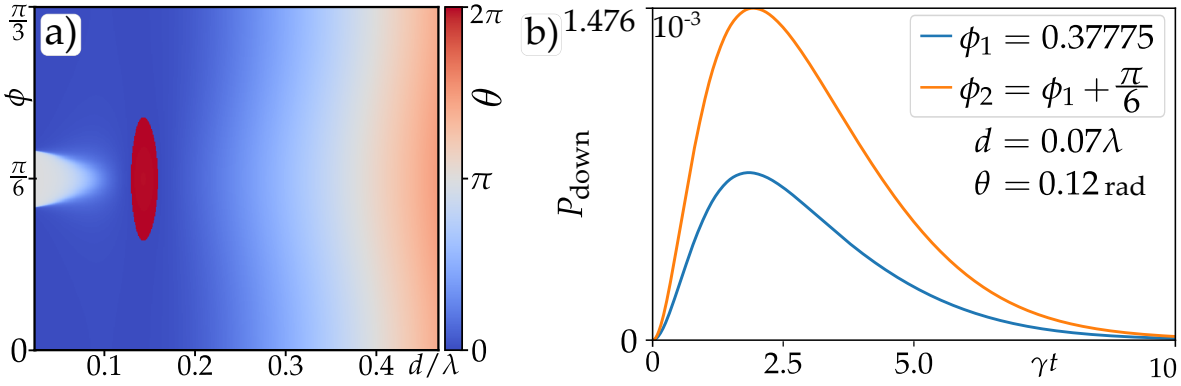

Figure A.1: The first plot (a) Shows the depencande of the Phase in the loop for an equilateral triangle. The angle ϕ measures the orientation of the dipoles with respect to the x-axis. Care must be taken, as multiple combinations of d/λ and ϕ can lead to the same θ but result in different evolutions, as seen in (b). The second plot (b) shows the evolution of a classical state which is initially on the left arm, exactly like in [1].

simple explanation for this is that the Hamiltonian for the atomic system is not hermitian. Therefore, mathematically, no chirality is possible in this system, and this kind of control is not possible.

A.2 Diagonalization

The Figure A.2 shows, that the matrix $(V)_{\alpha\beta}$ defined in section 2.4.2 for a chain of N atoms can be diagonalized in a good approximation. The matrices in k-space are mainly diagonal with a defect in the off-diagonal corners. The same holds for the matrix $(\Gamma)_{\alpha\beta}$. The larger the system, the better the approximation.

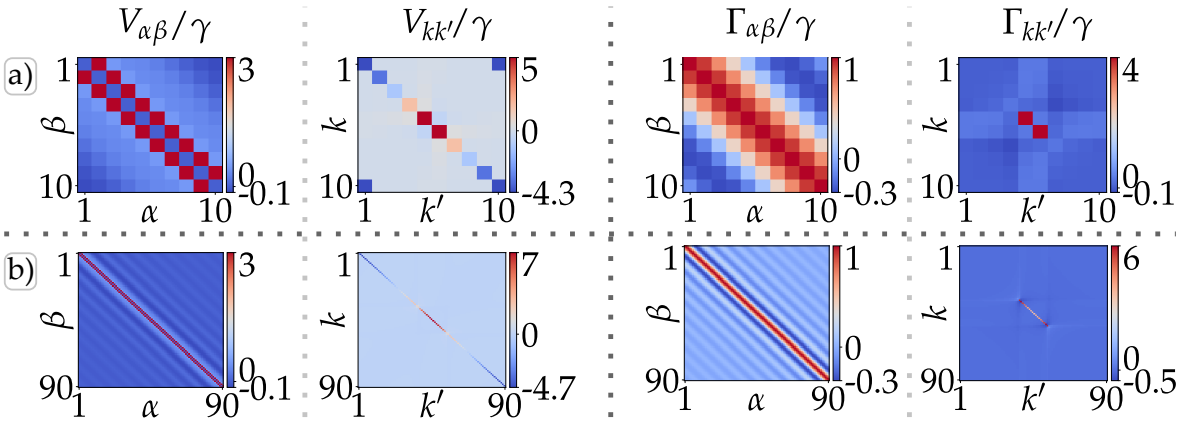

Figure A.2: a) Chain of $N = 10$ atoms. **b)** Chain of $N = 90$ atoms. The atomic dipoles are aligned and perpendicular to the chain. The interaction matrix $(V)_{\alpha\beta}$ and $(\Gamma)_{\alpha\beta}$ are displayed in units of γ. Left side in real space and right side in k-space.

Bibliography

[1] A. Bottarelli, M. Frigerio, and M. G. A. Paris, *Quantum routing of information using chiral quantum walks*, 2023.

[2] S. J. Masson and A. Asenjo-Garcia, "Universality of dicke superradiance in arrays of quantum emitters", Nature Communications **13**, 2284 (2022).

[3] A. Asenjo-Garcia, J. D. Hood, D. E. Chang, and H. J. Kimble, "Atom-light interactions in quasi-one-dimensional nanostructures: a green's-function perspective", Physical Review A **95**, 033818 (2017).

[4] J. A. Needham, I. Lesanovsky, and B. Olmos, "Subradiance-protected excitation transport", New Journal of Physics **21**, 073061 (2019).

[5] M. Cech, I. Lesanovsky, and B. Olmos, "Dispersionless subradiant photon storage in one-dimensional emitter chains", Physical Review A **108**, Published 21 November 2023, 10.1103/PhysRevA.108.L051702 (2023).

[6] M. O. Scully, "Single photon subradiance: quantum control of spontaneous emission and ultrafast readout", Physical Review Letters **115**, 243602 (2015).

[7] A. Asenjo-Garcia, M. Moreno-Cardoner, A. Albrecht, H. J. Kimble, and D. E. Chang, "Exponential improvement in photon storage fidelities using subradiance and "selective radiance" in atomic arrays", Phys. Rev. X **7**, 031024 (2017).

[8] H.-P. Breuer and F. Petruccione, "Concepts and methods in the theory of open quantum systems", Reviews of Modern Physics **77**, 175–217 (2002).

[9] D. Manzano, "A short introduction to the lindblad master equation", AIP Advances **10**, 10.1063/1.5115323 (2020).

[10] R. H. Dicke, "Coherence in spontaneous radiation processes", Phys. Rev. **93**, 99–110 (1954).

[11] M. Gross and S. Haroche, "Superradiance: an essay on the theory of collective spontaneous emission", Physics Reports **93**, 301–396 (1982).

[12] P. Lodahl, A. F. van Driel, I. Nikolaev, X. Brokmann, D. V. Sergent, M. Besombes, J. M. Gerard, D. M. Smith, W. L. Vos, and H. J. Sandoghdar, "Controlling the dynamics of spontaneous emission from quantum dots by photonic crystals", Nature **430**, 654–657 (2004).

[13] O. Rubies-Bigorda and S. F. Yelin, "Superradiance and subradiance in inverted atomic arrays", Phys. Rev. A **106**, 053717 (2022).

[14] J. Bohnet, Z. Chen, J. Weiner, D. Meiser, M. J. Holland, and J. K. Thompson, "A steady-state superradiant laser with less than one intracavity photon", Nature **484**, 78–81 (2012).

[15] B. Bellomo, G. L. Giorgi, G. M. Palma, and R. Zambrini, "Quantum synchronization as a local signature of super- and subradiance", Phys. Rev. A **95**, 043807 (2017).

[16] R. Grimm, M. Weidemüller, and Y. B. Ovchinnikov, "Optical dipole traps for neutral atoms", in , Vol. 42, edited by B. Bederson and H. Walther, Advances In Atomic, Molecular, and Optical Physics (Academic Press, 2000), pp. 95–170.

[17] T. Bienaimé, N. Piovella, and R. Kaiser, "Controlled dicke subradiance from a large cloud of two-level systems", Phys. Rev. Lett. **108**, 123602 (2012).

[18] F. Bloch, "Über die quantenmechanik der elektronen in kristallgittern", Zeitschrift für Physik **52**, 555–600 (1929).

[19] X. Shu, Q. Zhong, K. Hong, O. You, J. Wang, G. Hu, A. Alù, S. Zhang, D. N. Christodoulides, and L. Chen, "Chiral transmission by an open evolution trajectory in a non-hermitian system", Light: Science & Applications **13**, 65 (2024).